17 Physical Systems Biology and non-equilibrium Soft Matter

C.M. Aegerter, D. Assmann, D. Eder (since July 2012), G. Ghielmetti, F. Lanfranconi (since February 2013), U. Nienhaus, and T. Schluck

in collaboration with: Institute of Molecular Life Sciences (K. Basler, T. Aegerter-Wilmsen, C. Lehner, S. Luschnig, D. Brunner), ETH Zürich (E. Hafen, P. Koumoutsakos), EPF Lausanne (P. Renaud), University of Lausanne (S. Bergmann), Biozentrum Basel (M. Affolter), University of Strasbourg (N. Rivier), University of Fribourg (A. Jazwinska), University of Konstanz (G. Maret, W. Bührer, T. Sperling, N. Isert), New York University (C.C. Maass), Deutsches Luft- und Raumfahrtzentrum (M. Sperl), University of Twente (A. Mosk), Universite Joseph Fourier Grenoble (S. Skipetrov, F. Graner), Technion Haifa (E. Akkermans).

Work in the group of physical systems biology and non-equilibrium soft-matter is concerned with the study of developmental biology using physical techniques, light transport in turbid media and the dynamics of systems inherently out of thermodynamic equilibrium. In turbid media, we are studying both fundamental problems, such as the transition to Anderson localization with increasing disorder in the scattering medium, as well as application oriented problems such as the development of imaging methods behind turbid structures. In developmental biology, we are partly using these imaging capabilities to study developmental processes in living organisms, and are also concerned with the influence of mechanical forces on developmental processes, e.g. growth. Finally in non-equilibrium systems, we are studying the dynamics of granular gases and foams, in particular in the presence of levitation, such that effects due to gravity can be eliminated and the generic process can be studied. In the last year, we have made considerable progress in several of these areas, two of which are discussed in detail below. These subjects concern the coarsening dynamics of levitated foams and the mechanical control of growth of the wing imaginal disc of Drosophila.

17.1 Coarsening Dynamics in Levitated Foams

Due to the immiscibility of air bubbles and water, a foam is inherently unstable and presents a generic out of equilibrium system [1]. When a foam is left alone, the final state will consist of a separated air and liquid volume. The process leading to this equilibration is called coarsening. In most foams, this process is superimposed by a flow of liquid due to gravity, which will lead to the separation much faster, but this is an inhomogeneous process, due to the stratification in density as a function of height called drainage [2]. Therefore in order to study the process of coarsening, levitated foams are needed, which we achieve by the use of diamagnetic levitation in wa-

ter nitrogen mixtures in a strong magnetic field gradient [3, 4]. Using a superconducting solenoid, we can apply field up to 20 T onto a sample, leading to field gradients at the edge of the solenoid of the order of 100 T/m. This means that there is a levitation force proportional to $B\partial_z B$, which counteracts the gravitational force [5]. Given the diamagnetic susceptibility of water, the levitation force exactly cancels the gravitational force at an applied field of around 18 T [6]. Thus we can eliminate drainage in the dynamics of foams and purely study the coarsening process. This is of interest, since there are several predictions to the temporal behaviour of these dynamics, as well as a transition with increasing liquid content of the foam [7–9].

The coarsening process consists of a growth of larger bubbles on the expense of smaller ones by gas exchange between these bubbles holding different internal pressures. This (Laplace-)pressure Δp, is proportional to Δp, i.e. to the inverse of its radius, such that small bubbles preferentially blow up bigger bubbles. In dry foams the exchange of gas between bubbles takes place directly through the thin liquid films separating the bubbles[10]. This implies that the gas flow current density $j = \frac{dV}{Adt} \propto dr/dt \propto \Delta p \propto 1/r$. Here, A is the contact area of a bubble which is of order r^2 and V its volume. Solving this, one obtains that the average size of bubbles will increase with time as $\langle r \rangle \propto t^{1/2}$. This can also be derived more rigidly, as for instance done in [11], where strictly speaking the pressure difference between two different bubbles is considered.

When the bubbles are no longer in contact, i.e. at higher liquid fractions exceeding roughly 30% corresponding to the inverse structure of random closed packing, it can be surmised that the mechanism of gas exchange between bubbles will have to change and take place via gas diffusion in the liquid. Here, the diffusive current density $j \propto dr/dt$ will be determined
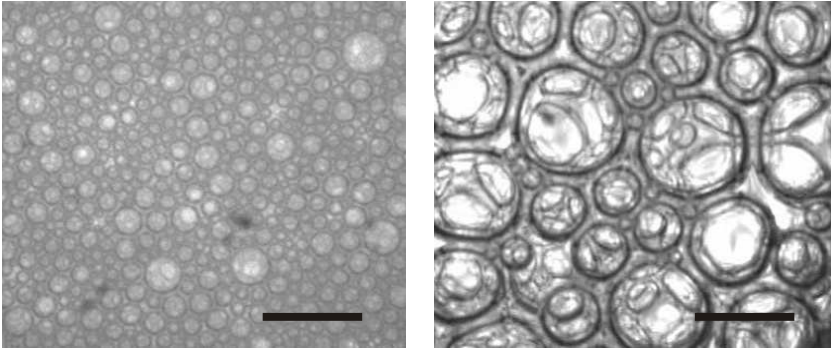
FIG. 17.1 – Images of the surface of the foam chamber showing the absolute size and polydispersity 10 min (left) and 152 min (right) after creation. The scale bars correspond to 1 mm.
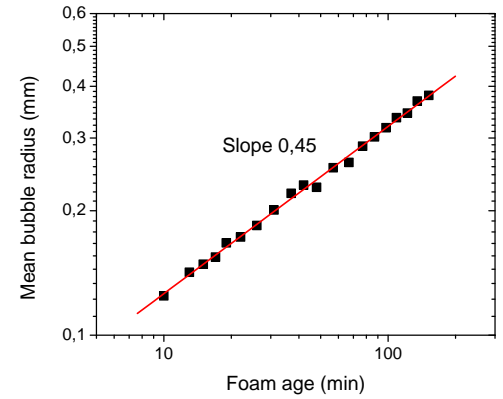

FIG. 17.2 – The mean bubble radius varies in time like $\langle r \rangle \propto t^{\beta}$ with $\beta = 0.45(5)$.

by the gradient of the concentration, i.e. the gradient in pressure difference. This means that we obtain $j \propto dr/dt \propto dp/dr$. Again using the fact that the pressure inside the bubbles is given by Laplace's law, we obtain $dr/dt \propto 1/r^2$ and hence a growth of the form $\langle r \rangle \propto t^{1/3}$. Again, this can be derived studying the detailed dynamics [7]. This qualitatively different type of coarsening is also known as Ostwald ripening and is for instance observed in the dynamics of the growth of inclusions in solids [12]. This transition has also been obtained in simulations of two-dimensional foams considering different liquid fractions[13]. Since levitated foams can be created with a varying amount of liquid and relative stability to drainage, these predictions
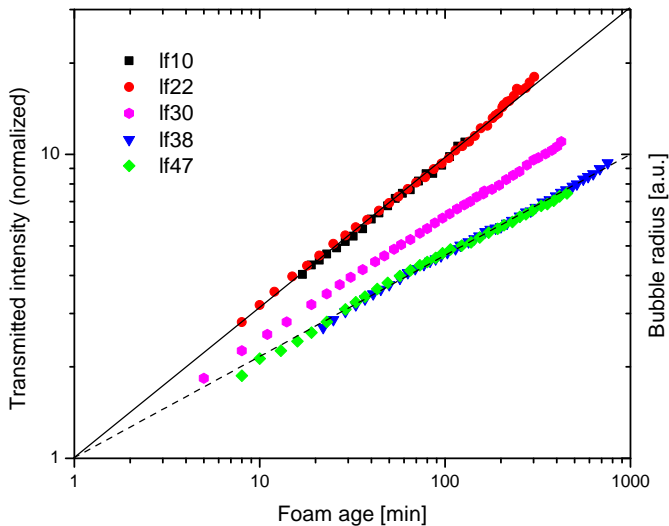

FIG. 17.3 – The bubble size determined via the optical transmittance as a function of foam age is shown for five different liquid fractions. The plot is on doubly logarithmic scales indicating power law dependence of the size with age. Straight lines with a slope of 1/2 (solid) and 1/3 (dashed) indicating the exponents of von Neumann and Ostwald dynamics are added for comparison.
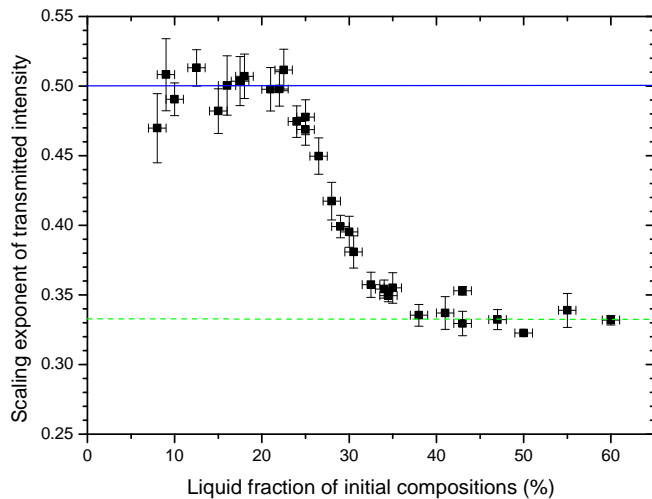
can thus be tested experimentally with our setup. The foams used in the experiments consist of water, sodium dodecyl sulfate (SDS) as a surfactant and N_2 gas. The water-SDS mixture and the gas are put in two separate syringes, which are connected through a thin tube [14]. An initial liquid fraction of 25% corresponds roughly to an effective liquid fraction of 30%. This can be estimated from the pressure exerted by the foam in the syringes. The polydisperse foam with an average bubble radius of $r_0 \simeq 100 \mu m$ (see Figures 17.1 and 17.2) thus created is then transferred to a sample-cell.

In order to determine the bubble size in the bulk of a three dimensional foam, we use the multiply scattered transmitted intensity through the sample. This intensity is given by Ohm's law, i.e. $T \propto l^*/L$ [15], where L is the thickness of the sample and l^* is the transport mean free path, characterizing the turbidity of the foam. The mean free path of light in the sample has been shown before to give a determination of the bubble size with $l^* \propto r$ [16] for the bulk of the three dimensional foam, since it basically corresponds to the size of a scatterer. Thus we obtain a measure of the bubble size by a determination of the average transmitted intensity, i.e. l^* with foam age, since both the sample thickness and the incident intensity are fixed. In Fig. 17.3, this dependence of l^* with foam age is shown for a set of foams with different liquid content [6]. As can be seen in this double logarithmic plot, all foams show a scaling behavior with a power law increase of bubble size with age, $r \propto t^{\beta}$. At lower liquid fraction, the data are in good agreement with those obtained directly from the surface bubbles shown in Fig. 17.2. For dry foams, this increase shows an exponent close to $\beta = 1/2$, whereas for wet foams shows $\beta = 1/3$. These exponents are the asymptotic dynamics of the theoretical predictions for foam dynamics in the dry and wet case, respectively[7, 8].

69

FIG. 17.4 – The bubble growth exponent, β, determined from measurements as those shown in Fig. 17.3 versus liquid fraction. The expectations from von Neumann dynamics, $\beta = 1/2$, and from Ostwald ripening, $\beta = 1/3$ are shown for comparison. The transition region between these two regimes is rather narrow at liquid fractions between 25 % and 35 %.

70

These results are summarized in Fig. 17.4, where the exponents fitted for all experiments within a large range of liquid fractions is plotted [6]. It can be clearly seen that below a liquid fraction of 25%, the exponents are all compatible with 1/2, whereas above an initial liquid fraction of 35%, they are all compatible with 1/3. Thus there is a clear transition in the coarsening behavior of the foams at a liquid fraction corresponding to the close packing of spheres. Both the transition as well as the values of the exponents are predicted by theory[7, 8].

[1] D. Weaire and S. Hutzler, *The Physics of Foams*, Oxford Univ. Press (1999).

[2] S.A. Koehler *et al.*, Phys. Rev. E **58**, 2097 (1998).

[3] W. Braunbeck, Z. Phys. **112**, 764 (1939).

[4] M.V. Berry and A.K. Geim, Europ. J. Phys. **18**, 307 (1997).

[5] C.C. Maass, N. Isert. G. Maret and C.M. Aegerter, Phys. Rev. Lett. **100**, 248001 (2008).

[6] N. Isert, G. Maret, C.M. Aegerter, EPJE to be published (2013).

[7] W. Ostwald, Z. Phys. Chem. **37**, 385 (1901); I.M. Lifshitz and V.V. Slyozov, J. Phys. Chem. Solids **19**, 35 (1961); C. Wagner, Z. Elektr. Inf.-Energietech. **65**, 581 (1961); A. J. Markworth, Metallography **3**, 197 (1970); W.W.Mullins, J. Appl. Phys. **59**, 1341 (1986).

[8] J. von Neumann, in *Metal Interfaces* (C. Herring ed.), 108 (1952).

[9] A. Saint-Jalmes, S. Marze, M. Safouane and D. Langevin, Microgravity sci. technol. **XVIII**, 5 (2006).

[10] J.Lambert *et al.*, Phys. Rev. Lett. **99**, 058304 (2007).

[11] R.D. MacPhearson and D.J. Srolovitz, Nature (London) **446**, 1053 (2007).

[12] A. Knaebel *et al.*, Europhys. Lett. **52**, 73 (2000).

[13] I. Fortuna *et al.* Phys. Rev. Lett. **108**, 248301 (2012)

[14] A. Saint-Jalmes, M.U. Vera and D.J. Durian, Europ. Phys. J. B **12**, 67 (1999).

[15] P. Sheng, *Introduction to Wave Scattering, Localization and Mesoscopic Phenomena*, Academic Press (1995).

[16] A.S. Gittings, R. Bandyopadhyay and D.J. Durian, Europhys. Lett. **65**, 414 (2004).

17.2 Mechanical regulation of growth in the Drosophila wing disc

The regulation of organ size is a fundamental unsolved question in developmental biology [1]. While a great body of knowledge has been accumulated over the last decades on the genetic control of biochemical pathways, several questions concerning organ growth, in particular that of its cessation, remain unanswered. Organ growth is widely studied on the example of the wing imaginal disc of Drosophila due to the availability of a host of genetic tools [2]. The wing disc is the larval precursor organ that turns into the wing of the adult fly during metamorphosis.

In the past, growth of the wing disc has mainly been studied by the induction of gene expression at early stages in a small number of cells and then studying the final outcome of the process at the end of the third instar stage shortly before metamorphosis [3]. However for a full understanding of the growth and development process, time-dependent studies that can be compared with theoretical models need to be performed. This is what we will describe in the following. Such an investigation has been difficult in the past due to the lack of imaging techniques for the wing disc inside living larvae, which we have developed over the last years [4]. In addition, we have further developed our computational models [5, 6] of the growth process in the wing disc to include not only a description of the elastic properties of the disc on a cell based level [7], but also comb-
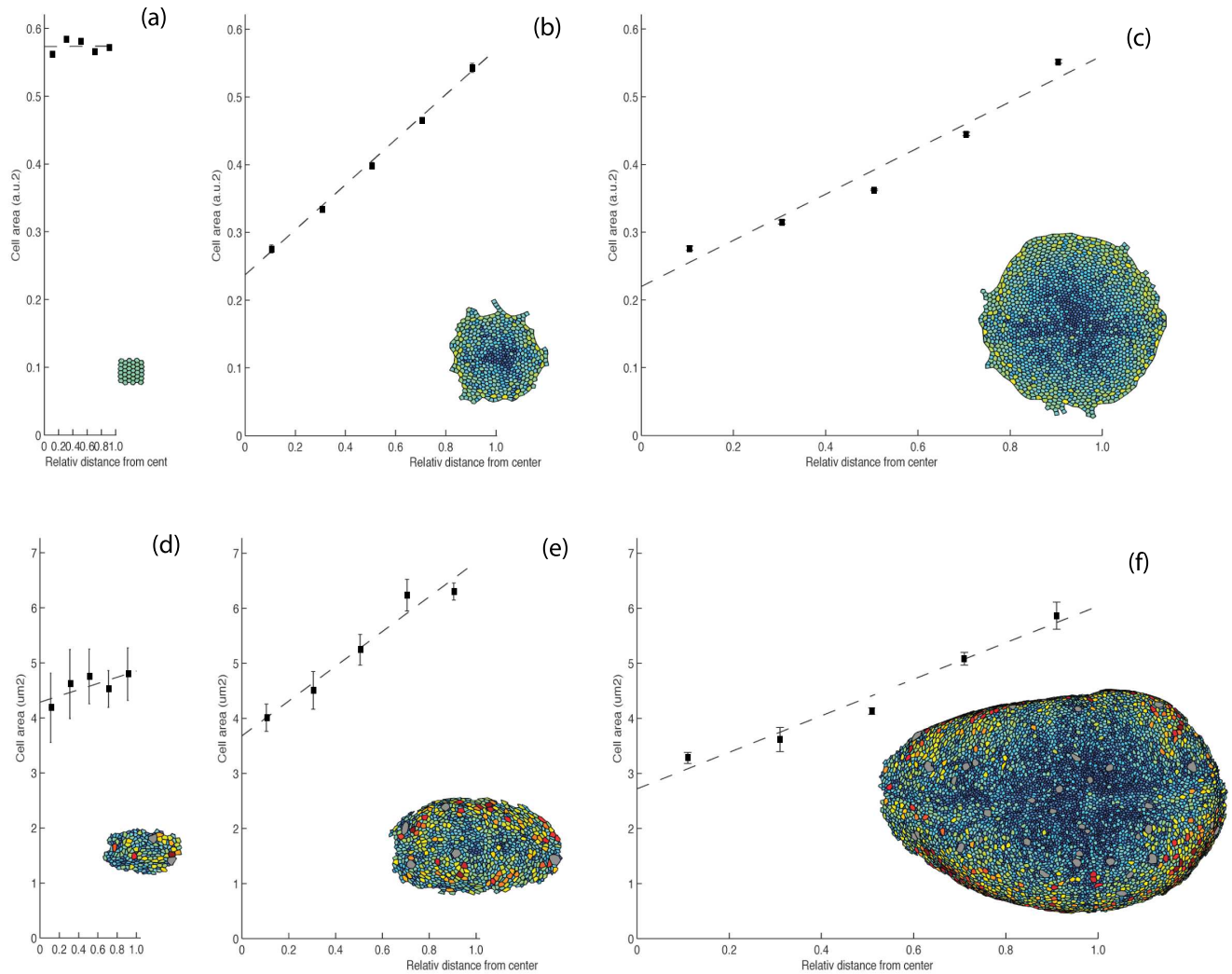
FIG. 17.5 – Comparison of predicted and measured cell area distributions. Our model predicts an initial build-up of a cell area gradient (a, b), which is flattened at later stages (c). The initial conditions (a) are compared with wing discs early in the third instar stage (d), the final simulated distributions (c) with late third instar discs (f). The pouches of the mid third instar discs (e) contain about 4 times less cells than those of the late third instar and are compared with simulated discs (b) that contain roughly the same factor less cells than the final simulated disc. The scale bar corresponds to 10 a.u. for the simulated and 25 μm for the experimental discs. Cells were colored according to their area, ranging from 0(blue) to 1.3(red) a.u.^{2} for the simulated and from 0(blue) to 16(red) μm^2 for the experimental discs. Grey cells are in mitosis and were excluded from the analysis.

ining this with the known key biochemical pathways [8, 9]. With this, we have a detailed model with which to compare to experimental results. The basic premise of the model is that mechanical feedback is used to regulate the growth of the tissue [5, 10, 11]. This means that the addition of material inside the tissue due to cell division leads to the acting of forces on the present cells. In the presence of elastic properties, these mechanical stresses can be stored in the tissue and lead to a change in growth rates of the tissue. In particular, it is assumed that compressed cells grow more slowly and stretched cells grow faster.

Using this feedback, the model can explain the cessation of growth when taking into account known biochemical pathways influencing growth as well.

The occurrence of such stresses has been inferred experimentally from birefringence measurements [12], as well as from a characterization of cell-cell interactions based on the proposition that local force balances yield the geometry of the cell shapes in the tissue [13]. Starting from experimental images of cell shapes, [13] solved the inverse problem of force balance, thus determining the local forces and showing that the compressional stress

strongly and negatively correlates with the apical area of a cell [13]. In addition, we have determined the local strain tensor has been determined for the tissue. It also shows radial tension in the periphery and compression in the center [8], as shown in Fig. 17.5. In addition to the measure shown in that figure, namely the apical cell area, we have also determined the direction of the deformation, which is tangential in the periphery and radial in the centre.

Using a combination of index matching, larval positioning and confocal microscopy, we are also able to image the entire developmental period of a wing disc within a single live larva [4]. This can be done with cellular resolution, as shown in Fig. 17.6, where the cell outlines are shown for a single wing disc during the time course of 120 hours covering all three larval instar stages. The individual cells can be identified and their apical area, number and topology can be determined for the different stages of development. For instance, we can determine the proliferation rate of cells at different times and correlate them with the forces acting on the cells in the tissue via the determination of the apical cell area. This is an indirect test of the assumption that growth is coupled to the mechanical stresses acting in the tissue. In fact, our detailed model [8] treats the mechanical feedback directly in this way in that the proliferation rate of a cell is given by its apical cell area. The experimental results regarding this are shown in Fig. 17.7, where during all stages of development, there is a clear dependence of the proliferation rate on mechanical force, i.e. apical cell area. This has also been observed in the growth of cell cultures [14].

Thus using in-vivo imaging and computational modelling, we have a full description of the growth process as well as of the forces acting on the tissue in these different stages, where both the distribution of cell areas in the tissue as a consequence of growth as well as the dependence of growth rate on cell area are in good agreement [8]. Finally, we can use in-vivo imaging to study external factor acting on the wing disc during development, which cannot be done using dissected tissues. Here, we have found additional evidence for the importance of mechanical forces on the development of the wing disc [4, 15]. At the time of maximal growth, during the late second instar and the beginning of the third, there are external tensional forces acting on the wing disc, as shown in Fig. 17.8. This again is in good agreement with the assumption of mechanical regulation of growth, In particular with the initial stages, where the biochemical growth factors are not yet fully developed.
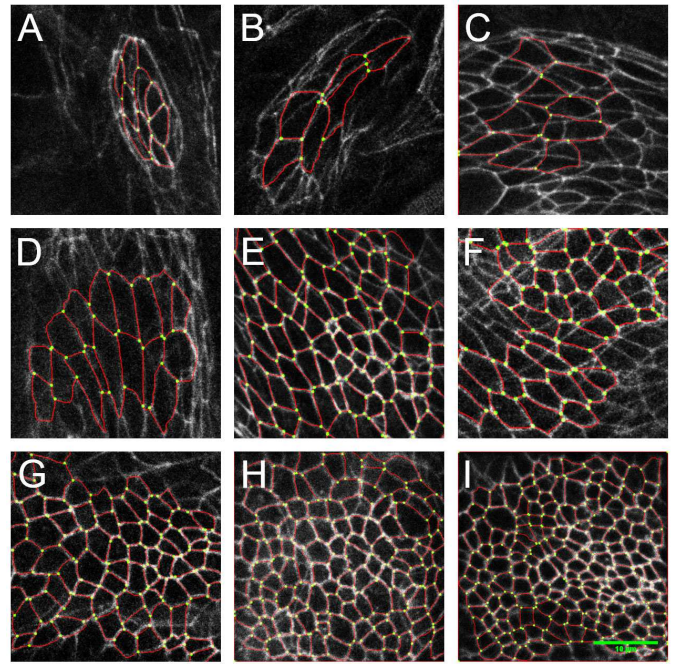

FIG. 17.6 – Cell junction outlines for the same wing disc as a function of time for nine different time points covering the whole of the developmental period spanning five days. The images correspond to time points of: A: 24 h, first instar; B: 32 h, second instar; C: 48 h; D: 56 h; E: 72 h; F: 80 h, third instar; G: 96 h; H: 104 h; and I: 120 h. The scale bar denotes 10 μm. Identified cell outlines are superimposed in red.
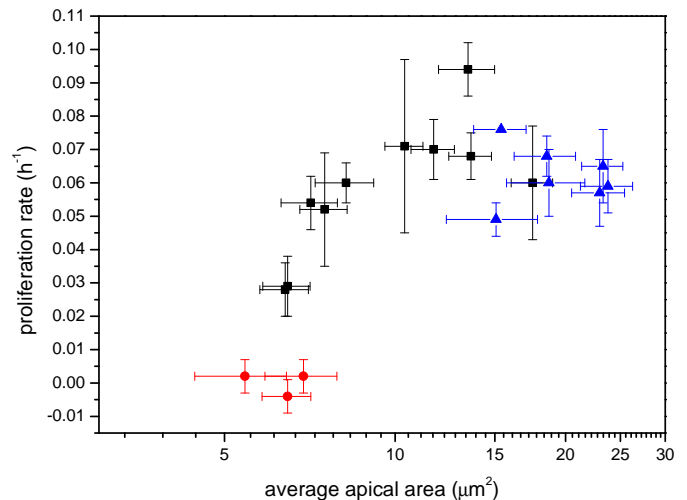

FIG. 17.7 – The correlation between the proliferation rate of cells in the wing disc and the average apical area of the cells for different times during development. Colors correspond to different instar stages: red first instar, blue second instar and black third instar.
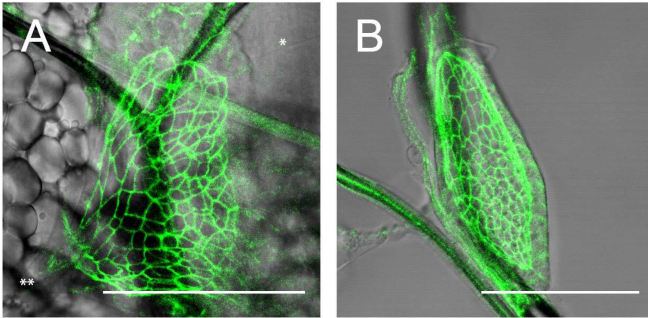
FIG. 17.8 – Images of a wing disc, where the apical cell outlines of the disc proper are marked by GFP fused to E-Cadherin. A: wing disc in vivo at the beginning of the third instar. In this image, several sources of mechanical force can be discerned. A tiny thread is attached to the wing disc on the posterior side (*). Also, the large muscle fiber between the wing, leg and haltere discs is clearly exerting a substantial force on the disc at (**). The cell outlines are correspondingly distorted. B: the same wing disc after dissection. Due to the dissection, the external force from the muscle fiber and the thread has been removed and the shape of the disc as well as that of the cell outlines has relaxed, showing a marked difference to A. The scale bar is 50μm.

[1] L. Wolpert, Development, Oxford Univ. Press (2007).

[2] A.D. Lander, Cell **144**, 955 (2011).

[3] M. Affolter, K. Basler, Nat Rev Genet. **8**, 663 (2007).

[4] U. Nienhaus, T. Aegerter-Wilmsen, and C.M. Aegerter, PLoS ONE **7**, e47594 (2012).

[5] T. Aegerter-Wilmsen, C.M. Aegerter, E. Hafen, and K. Basler, Mechanisms of Development **124**, 318 (2007).

[6] T. Aegerter-Wilmsen *et al.*, Development **137**, 499 (2010).

[7] R. Farhadifar, J.C. Röper, C. Aigouy, S. Eaton, and F. Jülicher, Curr Biol. **17**, 2095 (2007).

[8] T. Aegerter-Wilmsen *et al.*, Development **139** 3221 (2012).

[9] S. Dupont, *et al.* Nature **474**, 179 (2011).

[10] B.I. Shraiman, Proc Nat. Acad. Sci. USA **102**, 3318 (2005).

[11] L. Hufnagel, A.A. Teleman, H. Rouault, S.M. Cohen, and B.I. Shraiman, Proc Nat Acad Sci USA **104**, 3835 (2007).

[12] U. Nienhaus, T. Aegerter-Wilmsen, and C.M. Aegerter, Mechanisms of Development **126**, 942 (2009).

[13] S. Ishihara and K. Sugimura, J. Theor. Biol. **313**, 201 (2012).

[14] A. Puliafito *et al.*, Proc. Nat. Acad. Sci. USA **109**, 739 (2012).

[15] C. Dambly-Chaudiére, A. Ghysen, Y.N. Jan, and Y.L. Jan, Developmental Biology **113**, 288 (1986).